Respiratory Motion Correction in Emission Tomography Imaging

Mauricio Reyes, Grégoire Malandain, Pierre Malick Koulibaly, and Jacques Darcourt

***Abstract*— During an emission tomography exam of lungs, respiratory motion blurs the reconstructed image, which may lead to misinterpretations and imprecise diagnosis. Solutions like respiratory gating, correlated dynamic PET techniques, list-mode data based techniques and others have been tested with improvements over the spatial activity distribution in lungs lesions, but with the disadvantages of either requiring extra hardware or more expensive scanner systems, or discarding part of the acquired data. The objective of this study is to include a respiratory motion model in the image tomographic reconstruction process, which will allow to consider all the acquired data, without any additional requirement. To this end, we propose an extension of the MLEM reconstruction algorithm, in which we extend the probability matrix to take into account both the motion and the deformation of the voxels to be reconstructed. We present results from synthetic simulations incorporating real respiratory motion data, demonstrating the potential benefits of such an approach.**

I. Introduction

The motivation of this work is the early diagnosis of tumors in lungs with Emission Tomography (ET) imaging. However, the respiration motion blurs the reconstructed images, especially in lower areas, and this affects the detection of small tumors, or when detected, their localization or size measurements. Osman and colleagues reported mislocalizations of lesions observed by fusing positron emission tomography (PET) and computerized tomography (CT) [1]. Similarly, significant tumor displacements, mainly due to respiratory motion, has been observed in others studies (e.g [2], [3]). Nehmeh and colleagues also reported a significant lesion volume increase in reconstructed images without motion compensation [4].

To our knowledge, respiratory motion correction has been rarely addressed in the literature. In [5], a method of respiratory compensation was proposed: it supposes an homogeneous object cross-section magnification and displacement in the axial plane. This is however not realistic for our purpose since the displacements inside the thorax due to respiration are not homogeneous [6]. Others groups have focused their efforts in list-mode data. They include respiratory gating [4], or respiratory-correlated dynamic PET [7]. Respiratory gating techniques improve the quality of the reconstructed data by reducing the blurring effect around the tumor, but they require additional hardware (respiratory gating) and specific data acquisition modes (which is not always available), and discard part of the acquired data. Similarly to respiratory gating, others solutions have been proposed for brain imaging. In [8], the data is split in smaller subsets of projections according to the eventually detected motion. This is similar to [9] where the data are temporally fractionated, and the motion is detected by computing the cross correlation between sinograms. An other approach of motion detection in list-mode data is also investigated in [10]. However, the last above approaches are only applicable for a sudden motion of the imaged subject, but not for a continuous motion like the ones induced by the respiration or the heart beat. More interesting are the recent approaches described in [11], [12] where the motion correction scheme consists in repositioning the line-of-responses (LOR) (for a known motion). However, some non-valid positions may be reached by the motion-corrected LOR's, and this decreases the practical interest of these methods.

In this preliminary study, we propose a variation of the MLEM reconstruction algorithm in which we incorporate a motion model. This comes to modify the probability matrix to take into account not only the displacements of the voxels to be reconstructed but also their deformations. This approach is detailed in the next section. Some results are presented afterwards.

II. Method

A. Maximum Likelihood Expectation Maximization

First introduced in emission tomography by Shepp and Vardi [13], the MLEM algorithm is based on a *Poisson* model for the emission process. For a given emission element *b* the number of emissions f_b follows a Poisson law with mean λ_b. Besides, the projection matrix R (or called by some authors *system matrix* or *transition matrix*) gives the probability that a certain emission from voxel b is detected by the detector d (called *dexel* hereafter). Furthermore, the number of detections from dexel d (i.e., p_d) can be expressed in terms of the number of emissions f_b, as follows

$$p_d = \sum_{b=1}^{b=n} f_b R_{db}. \tag{1}$$

Equation (1) is important since it states the relationship between detections and emissions through the system matrix values. We are interested to find the mean value λ from the set of projections p. This can be done by searching the maximum likelihood of getting a set of measures p given an image λ

$$\hat{\lambda} = \arg\max_{\lambda}[P(p|\lambda)]. \tag{2}$$

[1]Mauricio Reyes and Grégoire Malandain are with the Epidaure team, INRIA, Sophia Antipolis. 2004, Route des Lucioles BP93 06902 France. Telephone: (+33)492387182. E-mail:

[2]Jacques Darcourt and Pierre Malick Koulibaly are with the nuclear medicine department, Centre Antoine Lacassagne. 33 Avenue de Valombrose 06189 Nice, France. Telephone: (+33)492031148. E-mail:

It can be shown (see [13] for more details) that maximization of (2) can be found by means of an iterative algorithm

$$\lambda_b^{<K+1>} = \frac{\lambda_b^{<K>}}{\sum_d R_{db}} \sum_d \frac{p_d R_{db}}{\sum_{b'} \lambda_{b'}^{<K>} R_{db'}}, \qquad (3)$$

where p_d stands for the number of detections of dexel d, λ_b is the mean number of emissions from voxel b, R_{db} is the probability that a particle emitted from voxel b is detected by the detector d and K stands for the iteration number.

B. Incorporating movement correction into MLEM

In list-mode based approaches, the motion correction consists in discarding the acquisition data that disagree spatially with a static reference. In this study, we use a known motion to estimate the contribution of a voxel b to be reconstructed to every dexel d.

We model the continuous motion by the spatial transformations $\varphi_t : \mathbb{R}^3 \mapsto \mathbb{R}^3$, where $\varphi_t(m)$ denotes the position of point m at time t. This motion is observed from time $t = 0$ to $t = T$ and is discretized into a finite set of transformations φ_i, for $i = 0 \dots I$. The contribution R_{db}^C of a voxel b to be reconstructed to a dexel d becomes the weighted sum of the contributions R_{db}^i of deformed voxels $\varphi_i(b)$ to d:

$$R_{db}^C = \sum_i w_i R_{db}^i. \qquad (4)$$

The weights w_i allow to take into account the kinetic of the motion: $w_i T$ represents the duration where φ_t can be effectively approximated by φ_i.

As a consequence, the matrix R^C may have more non-null elements than matrix R (see Eq. (1)), since a voxel b may be detected by more dexels d. Moreover, for a non-null R_{db}, we have $R_{db} \geq R_{db}^C$ since during its motion, a voxel b may go out the portion of space spanned by dexel d. With respect to the static case, Eq. (3) will then be more computationally expensive. We now explicit the calculation of the contributions R_{db}^i.

C. Computation of system matrix terms

The voxels that contribute to a dexel d are assumed to intersect a 3-D line that stemed from d. Let us denote by l_{db} the length of the intersection of this line with the emission element b. We thus define the contribution of b to d by

$$\text{static: } R_{db} = \frac{l_{db}}{\sum_{d'} l_{d'b}} \qquad \text{dynamic: } R_{db}^i = \frac{l_{db}^i}{\sum_{d'} l_{d'b}^i}. \qquad (5)$$

In the static case, we model the emissions elements as spheres inscribed in the voxel to be reconstructed to facilitate the calculation of Eq. (5): see Fig. 1a. The summation in the denominators of equation (5) acts as a normalization term.

If no deformations can be assumed for emission elements b during their motion, we could still have used the intersection of a line with a sphere for the computation of the contribution R_{db}^i. However, this will not be realistic. Indeed, it has been shown that the displacements in the thorax (due to the respiratory motion) present a non-linear and a non-homogeneous behavior [3], [6]. Thus, we have to consider also the deformations of b. When under motion, the element emission b will deform into $\varphi_i(b), i = 0 \dots I$. As a first order approximation, a deformed sphere is an ellipsoid. The contribution of b at state i to d, *i.e.* $\varphi_i(b)$, is then similarly defined as the length intersection of the line d with this ellipsoid (see Fig. 1b). We now detail the estimation of this ellipsoid.

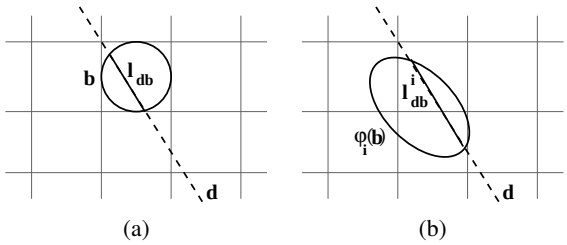

Fig. 1. The contribution of an emission element b to a dexel d represented by a dotted line is defined by the intersection (continuous line) of (a) a sphere with a line (static case) or (b) an ellipsoid (a deformed sphere) with a line (dynamic case).

Without loss of generality, the deformation φ (we omit here the subscripts t or i for the sake of simplicity), that transform the point (x, y, z) into $(x', y', z') = \varphi(x, y, z)$ can also be represented by a displacement vector field (DVF) $u(x, y, z)$ as follows

$$\varphi(x, y, z) = \begin{pmatrix} x' \\ y' \\ z' \end{pmatrix} = \begin{pmatrix} \varphi_x(x, y, z) = x + u_x(x, y, z) \\ \varphi_y(x, y, z) = y + u_y(x, y, z) \\ \varphi_z(x, y, z) = z + u_z(x, y, z) \end{pmatrix} \qquad (6)$$

The value of the determinant of $\nabla\varphi$ (also known as the Jacobian of φ) allows to determine whether the transformation φ induces locally an expansion ($|\nabla\varphi| > 1$), a contraction ($|\nabla\varphi| < 1$), or preserves the volumes ($|\nabla\varphi| = 1$). Moreover, the study of the matrix $\nabla\varphi$ allows to estimate the privileged directions of either contraction or dilation. Let us consider the singular value decomposition (SVD) of matrix $\nabla\varphi$, that is $\nabla\varphi = U\Sigma V^T$, where U and V are square and orthogonal matrices and $\Sigma = diag(\omega_1, \omega_2, \omega_3)$, with ω_i $(i = 1, 2, 3)$ the singular values of $\nabla\varphi$. It comes out that the columns of U are the eigenvectors of $\nabla\varphi\nabla\varphi^T$, and also give the preferred local deformation directions, while the ω_i are related to the magnitude of the deformations in the direction of the eigenvectors.

Consider now the center c_b of an emission element b, the study of $\nabla\varphi(c_b)$ results in these directions and magnitudes. If b is supposed to be spherical, then, by applying this simple deformation model to a sphere, it comes out that $\varphi(b)$ can be considered as an ellipsoid. This justifies the calculation of R_{db}^i by considering the intersections l_{db}^i of lines d with the ellipsoids $\varphi_i(b)$ (see Fig. 1b).

The modeling of the emissions elements as spheres that translate and deform locally according to a given DVF, represents a novel contribution in this work. Furthermore, calculations of the elements in the system matrix are faster

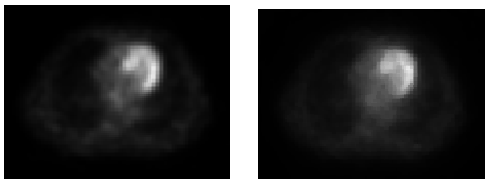

(a) COSEM (b) Modified MLEM

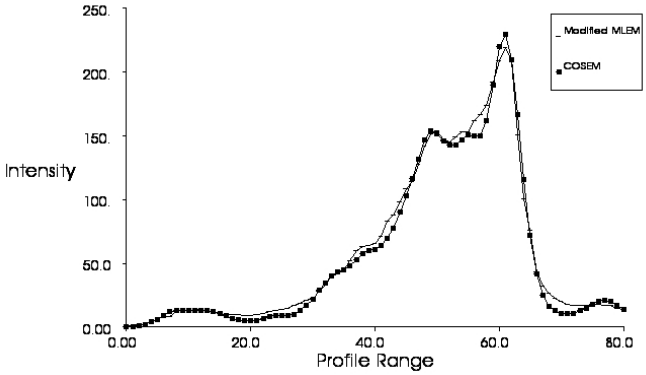

(c) Profile comparison

Fig. 2. Reconstructed images obtained with the COSEM algorithm (a), our modified MLEM algorithm (b) and a profile comparison along the x-axis between COSEM and our modified MLEM algorithm without respiratory motion correction (c).

(a) sagittal plane (b) axial plane (c) coronal plane

Fig. 3. Sagittal, axial and coronal cross-sections of the activity volume of the reference state. The lesion is modeled as a sphere with a radius of 1.5 cm (intensities were inverted for display purposes).

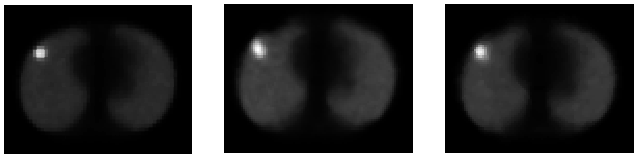

(a) Reference (b) Non-corrected (c) Corrected

Fig. 4. Reference activity map (a), and reconstructed images without (b) and with respiratory motion compensation (c).

than using classical methods of dexel-voxel intersection (e.g. Siddon algorithm [14]) utilized by others (see [15], [16] for examples of application).

III. Results

First, we were interested in somehow validating our reconstruction methodology that differs from existing ones (because of our probability matrix computation).

To that end, the reconstructed image of one patient sinogram data using the method presented in section II-C, considered in the static case, was compared with the reconstructed image obtained from a Millennium VG Scanner that uses COSEM (Coincidence-list-Ordered Sets Expectation Maximization)[17] as image reconstruction algorithm. Since COSEM uses an exact probability calculation, we can consider it as a reference. Fig. 2 shows the result obtained with COSEM and our modified MLEM method.

Fig. 2(c) displays a comparison of intensities profiles obtained with the two methods (COSEM and ours). This demonstrate clearly that our modeling of emission elements as spheres yields qualitatively similar results than the ones delivered by COSEM.

To now simulate the respiratory motion in an Emission Tomography study, we will build a model of the lungs (including a small lesion), deform it for each time state i, compute the sinograms for each time state i, and finally combine them.

As a 3-D model of the lungs, we use the thorax phantom *NCAT* (*NURBS-based cardiac torso*) [18]. In order to simulate a tumor lesion inside the lungs, a hot spot sphere of diameter 1.5 cm was added. Fig. 3 shows the activity image for the reference state. Then, to get a realistic model of the respiratory motion, two MR images of the thorax of a volunteer were acquired (at expiration and inspiration). Their non-rigid registration provides us with a volumic DVF u that we consider as a model of respiratory motion. By now performing an affine registration between this motion model and the 3-D model of the lungs, we can apply this respiratory motion to the 3-D model. The discretization of the motion is obtained by applying the DVFs $u_i = \frac{i}{I}u, i = 0 \dots I$ to the activity volume of the reference state. This yields $I+1$ activity volumes, each of them corresponding to a time state i. To now simulate an Emission Tomography acquisition of these activity volumes, the SimSET (*Simulation System for Emission Tomography*) library, which uses Monte Carlo techniques to model the physical process and instrumentation [19], is considered. Finally, the obtained sinograms are combined (through a weighted sum, with the weights w_i) into a single sinogram that simulates the acquisition of the 3-D models under a respiratory motion.

Fig. 4 shows a comparison between the reference activity map, and the reconstructions without and with respiratory motion compensation. A first and obvious observation is the larger size of the reconstructed lesion in the non-corrected reconstruction.

To better estimate this difference, we segment the lesion in the three images (with a fuzzy c-means classification). Isosurfaces were generated for the reference volume (*i.e.* expiration state) and for the non-corrected and corrected volumes (see Fig. 5).

This demonstrate the ability of the proposed method to better reconstruct the spatial distribution of the activity in the lesion. However, this depends on the segmentation of the lesion, which is very sensitive to the choice of the threshold because of the small size of the lesion.

Therefore, to better assess the quality of the reconstruction, we also provide a comparison between intensity profiles

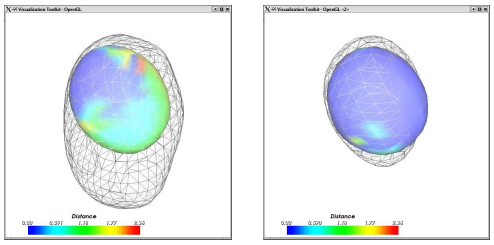

(a) Non-corrected (b) Corrected

Fig. 5. Comparison of the lesion volumes as seen in Fig. 3. Isosurfaces extracted from reconstructed images are rendered in wire-frame, while the one extracted from the reference is colored. The color indicates the distance between the two displayed surfaces, *i.e.* an error between the reference lesion and the reconstructed one.

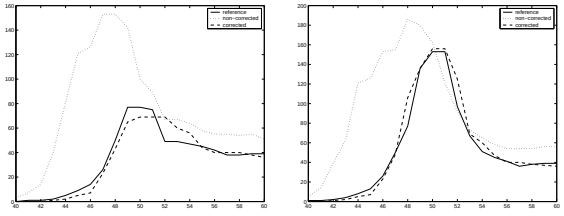

(a) x-coordinate: 34 (b) x-coordinate: 35

Fig. 6. Intensity profiles for axial slice 43 around the lesion area. After 20 MLEM iterations the corrected profiles (dashed line) show a close relationship with the reference profiles (continuous line) in comparison with the non-corrected profile (dotted line).

extracted from the reference activity map and the two reconstructed volumes. Fig. 6 shows two such profiles.

IV. Conclusion

During an emission tomography exam of lungs, respiratory motion blurs the reconstructed image, which may lead to misinterpretations and imprecise diagnosis, and if used for such a purpose, incorrect radiotherapy planning [20], [4], [3].

We proposed a novel reconstruction method that allows to incorporate a known motion, and in particular the respiratory motion, into the reconstruction process. As advantages, it does not require any additional hardware nor specific data storage mode (e.g. list-mode data), and can then be used for any Emission Tomography studies. Moreover, unlike gated approaches, all the acquisition data can be used.

The proposed method consists in a modification of the MLEM algorithm. More precisely, we modify the probability matrix (that summarizes the contribution of an emission element to a detector) computation to take into account not only the displacement of the emission elements but also their deformation under motion. To that end, we propose to model the emission element as a sphere (at rest) and as an ellipsoid (under motion).

Our preliminary results look promising and demonstrate the ability of the proposed method to compensate the reconstruction of simulated data for a known motion. In the future, we will now concentrate on the adaptation of this approach to real clinical data (CDET or PET data), where the respiratory motion of the imaged patient is unknown. Moreover, we plan to study carefully the sensitivity of our method with respect to the different parameters, and particularly the choice of the discrete states i.

References

[1] MM. Osman, C. Cohade, Y. Nakamoto, LT. Marshall, JP. Leal, and RL. Wahl. Clinically significant inaccurate localization of lesions with PET/CT: frequency in 300 patients. *J. Nucl. Med.*, 4(2):240–243, 2003.

[2] S. Shimizu, H. Shirato, K. Kagei, T. Nishioka, X. Bo, H. Dosaka-Akita, S. Hashimoto, H. Aoyama, K. Tsuchiya, and K. Miyasaka. Impact of respiratory movement on the computed tomographic images of small lung tumors in three-dimensional (3D) radiotherapy. *Int J Radiat Oncol Biol Phys.*, 46(5):1127–33, Mar 2000.

[3] Y. Seppenwoolde, H. Shirato, K. Kitamura, S. Shimizu, M. van Herk M, JV. Lebesque, and K. Miyasaka. Precise and real-time measurement of 3D tumor motion in lung due to breathing and heartbeat, measured during radiotherapy. *Int J Radiat Oncol Biol Phys.*, 53(4):822–34, July 2002.

[4] SA. Nehmeh, YE. Erdi, CC. Ling, KE. Rosenzweig, H. Schroder, SM. Larson, HA. Macapinlac, OD. Squire, and JL. Humm. Effect of respiratory gating on quantifying PET images of lung cancer. *J. Nucl. Med.*, 43(7):876–81, 2002.

[5] C.R. Crawford, K.F. King, C.J. Ritchie, and J.D. Godwin. Respiratory compensation in projection imaging using a magnification and displacement model. *IEEE Trans. on Med. Imag.*, 15(3):327–332, June 1996.

[6] L. Weruaga, J. Morales, L. Núñez, and R. Verdú. Estimating volumetric motion in human thorax with parametric matching constraints. *IEEE Trans. Med. Imag.*, 22(6):766–772, June 2003.

[7] SA. Nehmeh, YE. Erdi, KE. Rosenzweig, H. Schroder, SM. Larson, OD. Squire, and JL. Humm. Reduction of respiratory motion artifacts in PET imaging of lung cancer by respiratory correlated dynamic PET: Methodology and comparison with respiratory gated PET. *J. Nucl. Med.*, 44(10):1644–1648, 2003.

[8] Y. Picard and CJ. Thompson. Motion correction of PET images using multiple acquisition frames. *IEEE Trans Med Imag.*, 16(2):137–44, April 1997.

[9] C. Pellot-Barakat, M. Ivanovic, A. Herment, K. Erlandsson, and D. K. Shelton. Detection of motion in hybrid PET/SPECT imaging based on the correlation of partial sinograms. *IEEE Trans. Med. Imag.*, 20(10):1072–1083, Oct. 2001.

[10] G.J. Klein, B.W. Reutter, E.H. Botvinick, T.F. Budinger, and R.H. Huesman. Fine-scale motion detection using intrinsic list mode PET information. In *MMBIA01*, pages 71–78, 2001.

[11] K. Thielemans, S. Mustafovic, and L. Schnorr. Image reconstruction of motion corrected sinograms. In *IEEE Medical Imaging Conf.*, 2003.

[12] A. Rhamim and P. Bloomfield. Motion correction in histogram-mode and listmode EM reconstructions. In *IEEE MIC*, 2003.

[13] L. Shepp and Y. Vardi. Maximum likelihood reconstruction for emission tomography. *IEEE Trans. Med. Imag.*, 1(2):113–122, 1982.

[14] R. L. Siddon. Fast calculation of the exact radiological path for a three-dimensional CT array. *Med. Phys.*, 12:252–255, 1985.

[15] AJ. Reader, S. Ally, F. Bakatselos, R. Manavaki, RJ. Walledge, AP. Jeavons, PJ. Julyan, S. Zhao, DL. Hastings, and J. Zweit. One-pass list-mode EM algorithm for high resolution 3D PET image reconstruction into large arrays. *IEEE T. Nucl. Sci*, 49:693–699, 2002.

[16] G. T. Herman and D. Odhner. Performance evaluation of an iterative image reconstruction algorithm for positron emission tomography. *IEEE Trans. Med. Imag.*, 10(3):336–346, September 1991.

[17] R. Levkovitz, D. Falikman, M. Zibulevsky, A. Ben-Tal, and A. Nemirovski. The design and implementation of COSEM, an iterative algorithm for fully 3-D listmode data. *IEEE Trans Med Imaging*, 20(7):633–42, July 2001.

[18] W.P. Segars. *Development of a new dynamic NURBS-based cardiac-torso (NCAT) phantom*. PhD thesis, The University of North Carolina, 2001.

[19] RL. Harrison, SD. Vannoy, DR. Haynor, SB. Gillispie, MS. Kaplan, and TK. Lewellen. Preliminary experience with the photon history generator module of a public-domain simulation system for emission tomography. *Conf. Rec. IEEE Nucl. Sci. Symp.*, pages 1154–1158, 1993.

[20] MM.Osman, C. Cohade, Y. Nakamoto, and RL. Wahl. Respiratory motion artifacts on PET emission images obtained using ct attenuation correction on PET-CT. *J. Nucl. Med.*, 30(4):603–6, 2003.